Simulation and Implementation of Power Control Strategy Grid Connected Photovoltaic System

YOUSRY ATIA[3], M.M. SALEM[2,3] AREF ELIWA[3]AND MOHAMED ZAHRAN[1,3]

1. Jazan University, Faculty of Engineering, Electrical Eng. Dept., KSA, mzahran@jazanu.edu.sa, mbazahran_2007@yahoo.com
2. Taif University, Faculty of Engineering, Electrical Eng. Dept., KSA, masalem32@yahoo.com
3. Electronics Research Institute, National Research Center Building, El-Tahrir St., Dokki, 12311-Giza, Egypt, yousry_atia@yahoo.com

Abstract: - This paper introduces a direct power control strategy for a grid-connected voltage-source inverter. The proposed control strategy is implemented in the stationary reference frame without the necessity of the synchronous d-q transformation. The proposed control strategy based on the deadbeat current control technique and the relations between the grid currents and the instantaneous active and reactive power in the stationary reference frame. Then, the required inverter voltage in α-β reference frame is calculated directly based on instantaneous errors of active and reactive power. For its advantages, space vector modulation (SVM) is chosen to generate the VSI gating signals. Due the simplicity of the proposed control strategy, a fixed point microcontroller is used for control implementation. Extensive simulation and experimental results are provided which confirm the validity of the proposed control technique.

Keywords: *Photovoltaic, Renewable Energy, Inverters, Direct power control, deadbeat control, VSI, grid connected systems.*

1. Introduction

Recently, renewable energy sources have more attention of researchers and investors. Among the available renewable energy sources, the photovoltaic (PV) is considered the most promising technology especially in distributed generation systems (DGS). Distributed generation generally refers to small-scale (typically 1 kW – 50 MW) electric power generators that produce electricity at a site close to customers or that are tied to an electric distribution system [1]. In the grid-connected mode, maximum power is extracted from the PV system to supply maximum available power into the grid. Single-stage and two-stage grid-connected systems are commonly used topologies in single- and three-phase PV applications [2-5]. In a single-stage grid-connected system, the PV system utilizes a single conversion unit (dc/ac power inverter). However, to fulfill grid requirements, such a topology requires either a step-up transformer or a PV array with a high dc voltage. On the other hand, a two-stage grid-connected PV system utilizes two conversion stages; a dc/dc converter for boosting and conditioning the PV output voltage and tracking the maximum power point (MPP), and a dc/ac inverter for interfacing the PV system to the grid. In such a topology, a high-voltage PV array is not essential, because of the dc voltage boosting stage. Single-stage inverters have gained attention, especially in low voltage applications.

The conventional voltage source inverter (VSI) is the most commonly used interface unit in grid-connected PV system technology due to its simplicity and availability [6]. Control of VSI can be divided into indirect and direct control strategies. The indirect control is characterized by a voltage modulator (such as space vector modulation SVM or sinusoidal PWM) which computes the on/off times of inverter switches along a switching period through the evaluation of the voltage reference. This voltage reference is produced by the current controllers, which considers the inverter as a continuous voltage source. On the other hand, the direct control technique is aimed to control the instantaneous active and reactive powers and obtains a direct relationship between behavior of active and reactive power and the inverter output voltage vector.

The commonly used method of indirect power control is the voltage oriented control (VOC). VOC is based on the current vector orientation with respect to the grid voltage vector. In this technique, the line currents are decoupled into active and reactive power components in the d-q reference frame. Two PI controllers are used to control the decoupled components of the line currents to achieve indirect power control. VOC provides good transient behavior and PI current controller ensures zero steady state error. Besides its complex algorithm, one main drawback for this control scheme is that the performance relies highly on the tuning of the PI controller parameters. While direct power control (DPC) is based on the instantaneous active and reactive power control. In DPC, there are no internal current control loops and no PWM modulator, because the inverter switching states are directly selected by a look-up table based on the instantaneous errors between the commanded and measured values of the active and reactive powers. Compared to VOC, DPC has a simpler algorithm, no current control loops, no coordinate transformation, no separate PWM voltage modulator, and it has better dynamics performance. On the other hand, variable and higher switching frequency are the well-known disadvantages of the DPC scheme. This problem can be solved by space voltage modulation technique. SVM modulator based on a predictive power model was developed in [7-9]. The method, however, was implemented in the synchronous reference frame, which necessitates the angular information of network voltage and the synchronous coordinate transformations. A similar DPC scheme combining SVM and predictive approach was designed in [10]. A similar work was developed by the authors based on direct power transfer and was published in [17].

The present paper introduces design and implementation of deadbeat direct power control technique to control active and reactive power injected to the utility grid in grid-connected distributed power generated system. Proposed space vector modulator (PSVM) is used to output inverter vectors under a constant-switching-frequency operation.

2. Grid Connected System Modelling

2.1 Grid-Connected DC/AC Inverter System

The grid connected inverter system is composed of three phase two-levels inverter connected to the utility grid via 3-phase smoothing inductance (L) and 3-phase transformer. The system is connected to photovoltaic system to fed utility grid with power from this renewable energy source as shown in Fig. 1.

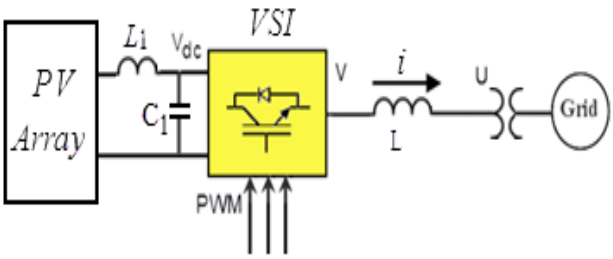

Figure 1, Grid connected DC/AC inverter system.

2.2 Grid Connected Inverter Modeling

Considering the grid supply and the output from a grid connected dc–ac inverter as an ideal voltage sources, Fig. 2 shows the simplified equivalent circuit of ac side of the inverter in αβ-reference frame.

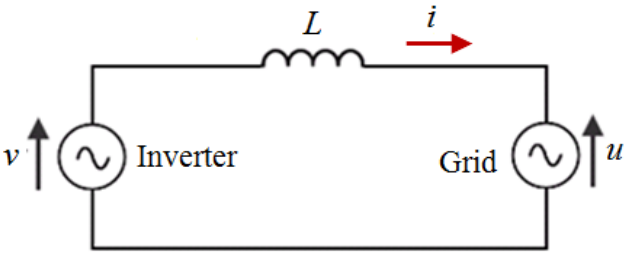

Figure 2, Equivalent circuit of grid-connected inverter.

2.2.1. The proposed system model in α-β reference frame

Considering the grid supply is an ideal voltage source, neglecting resistance (r) of the smoothing inductor, the relationship between the inverter output voltage (v) and the grid voltage (u) in α-β reference frame can be given by:

$$\begin{bmatrix} v_\alpha(t) \\ v_\beta(t) \end{bmatrix} = \begin{bmatrix} u_\alpha(t) \\ u_\beta(t) \end{bmatrix} + L\frac{d}{dt}\begin{bmatrix} i_\alpha(t) \\ i_\beta(t) \end{bmatrix} \quad (1)$$

The inverter vector can be expressed in discrete form as:

$$\begin{bmatrix} v_\alpha(k) \\ v_\beta(k) \end{bmatrix} = \begin{bmatrix} u_\alpha(k) \\ u_\beta(k) \end{bmatrix} + \frac{L}{T}\begin{bmatrix} i_\alpha(k+1)-i_\alpha(k) \\ i_\beta(k+1)-i_\beta(k) \end{bmatrix} \quad (2)$$

On the basis of the dead beat control scheme [11-12], and to make the actual current follows the reference current, the following relations are satisfied:

$$\begin{bmatrix} i_\alpha(k+1) \\ i_\beta(k+1) \end{bmatrix} = \begin{bmatrix} i_{\alpha ref}(k) \\ i_{\beta ref}(k) \end{bmatrix} \quad (3)$$

As a consequence, by substituting (3) into (2), (2) can be written in the following form:

$$\begin{bmatrix} v_\alpha(k) \\ v_\beta(k) \end{bmatrix} = \begin{bmatrix} u_\alpha(k) \\ u_\beta(k) \end{bmatrix} + \frac{L}{T} \begin{bmatrix} i_{\alpha ref}(k) - i_\alpha(k) \\ i_{\beta ref}(k) - i_\beta(k) \end{bmatrix} \quad (4)$$

Where:

T is the sampling period of the discrete system.

The grid active and reactive power can be calculated in α-β reference frame as [13]:

$$\begin{bmatrix} P(k) \\ Q(k) \end{bmatrix} = \frac{3}{2} \begin{bmatrix} u_\alpha(k) & u_\beta(k) \\ u_\beta(k) & -u_\alpha(k) \end{bmatrix} \begin{bmatrix} i_\alpha(k) \\ i_\beta(k) \end{bmatrix} \quad (5)$$

The current components in α-β reference frame can be obtained from (5) as:

$$\begin{bmatrix} i_\alpha(k) \\ i_\beta(k) \end{bmatrix} = \frac{2}{3(u_\alpha^2(k) + u_\beta^2(k))} \begin{bmatrix} u_\alpha(k) & u_\beta(k) \\ u_\beta(k) & -u_\alpha(k) \end{bmatrix} \begin{bmatrix} P(k) \\ Q(k) \end{bmatrix} \quad (6)$$

Also reference current can be expressed as:

$$\begin{bmatrix} i_{\alpha ref}(k) \\ i_{\beta ref}(k) \end{bmatrix} = \frac{2}{3(u_\alpha^2(k) + u_\beta^2(k))} \begin{bmatrix} u_\alpha(k) & u_\beta(k) \\ u_\beta(k) & -u_\alpha(k) \end{bmatrix} \begin{bmatrix} P_{ref}(k) \\ Q_{ref}(k) \end{bmatrix} \quad (7)$$

Substitution from (6) and (7) into (4), (4) can be written as follows:

$$\begin{bmatrix} v_\alpha(k) \\ v_\beta(k) \end{bmatrix} = \begin{bmatrix} u_\alpha(k) \\ u_\beta(k) \end{bmatrix} + \frac{L}{T} \frac{2}{3(u_\alpha^2(k) + u_\beta^2(k))} \begin{bmatrix} u_\alpha(k) & u_\beta(k) \\ u_\beta(k) & -u_\alpha(k) \end{bmatrix} \begin{bmatrix} P_{ref}(k) - P(k) \\ Q_{ref}(k) - Q(k) \end{bmatrix} \quad (8)$$

$$\begin{bmatrix} v_\alpha(k) \\ v_\beta(k) \end{bmatrix} = \begin{bmatrix} u_\alpha(k) \\ u_\beta(k) \end{bmatrix} + \frac{2L}{3T u_s^2(k)} \begin{bmatrix} u_\alpha(k) & u_\beta(k) \\ u_\beta(k) & -u_\alpha(k) \end{bmatrix} \begin{bmatrix} \Delta P(k) \\ \Delta Q(k) \end{bmatrix} \quad (9)$$

Where:

$$u_s^2(k) = u_\alpha^2(k) + u_\beta^2(k)$$

Using (9), the required inverter voltage in α-β reference frame can be calculated directly based on instantaneous errors of active and reactive power. This voltage is able to clear the power errors by the deadbeat at the end of the next sample.

From (9), the controller simplicity is clear. The control action just includes evaluating two simple algebraic equations in each sampling period that can be easily implemented using fixed point microcontroller. Fig.3 shows the block diagram of the proposed control system. In Fig. 3 the reference power P_{ref} is obtained from maximum power point tracking (MPPT) controller whereas the reactive power reference Q_{ref} is set to zero for unity power factor operation. Using Clark transformation, the three phase voltage and current signals are converted to two orthogonal signals [14]. From (5), the injected active and reactive power can be calculated, and from (9), the inverter voltage in αβ reference frame (v_α, v_β) can be calculated.

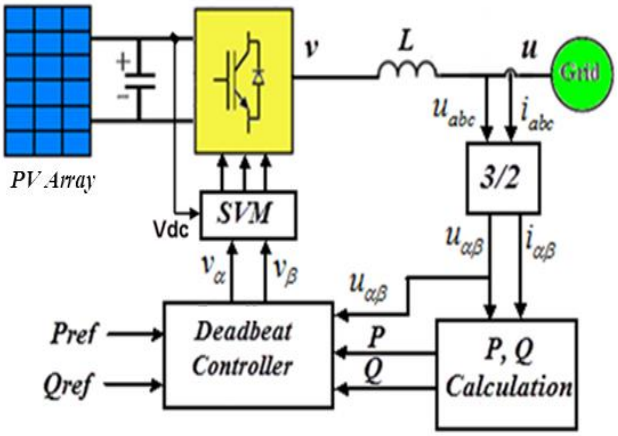

Figure 3, Block diagram of the proposed control system.

The inverter gating signals that control the VSI to generate the required voltage can be generated using one of the PWM generating techniques as sinusoidal pulse width modulation (SPWM), hysteresis PWM, or space vector pulse width modulation (SVPWM). Space vector modulation (SVM) is chosen to generate the VSI pulses for its advantages as more efficiency in using dc voltage, less output harmonic contents, and it has constant switching frequency for ease of filtering purpose. So, (9) is used to generate PWM signals for VSI using SVM technique.

A three-phase two-level inverter provides eight possible switching states, made up of six active states (v1-v6), and two zero switching states (v0,v7). Any reference vector V_s can be represented in α-β-plane as:

$$V_s = v_\alpha + jv_\beta = |V_s| \angle \theta \quad (10)$$

Where $|V_s| = \sqrt{v_\alpha^2 + v_\beta^2}$, $\theta = \tan^{-1} \frac{v_\beta}{v_\alpha}$

Since VSI cannot instantaneously generate V_S, the space-vector PWM principle consists in producing T-

periodic voltage whose average value equals to V_S. In sector number (n), SVM generates V_n during period t_1, generates V_{n+1} during period t_2 and generates v_0/v_7 during period t_0.

Where: $T = t_1 + t_2 + t_0$.

General expressions for these times can be written in a unified way as [15]:

$$t_1 = \frac{\sqrt{3}V_s T}{V_{dc}} \sin(\frac{\pi}{3} - \theta_1) \quad (11)$$

$$t_2 = \frac{\sqrt{3}V_s T}{V_{dc}} \sin\theta_1 \quad (12)$$

$$t_0 = T_s - t_1 - t_2 \quad (13)$$

Where:

$$\theta_1 = \theta - (n-1)*\frac{\pi}{3} \ , \ 0 < \theta_1 \le \pi/3$$

3. Simulation results

Simulation model of three-phase grid connected system is built using MatLab/Simulink environment to verify the controller operation. The simulated system parameters are given in Table 1.The simulation is carried out in two phases; steady-state phase and transient operation phase. Fig. 4 shows the MatLab/Simulink model of the proposed system.

Table 1, System parameters for simulation and experimental tests

DC bus voltage	113V
Transformer turns ratio	36/220 V
Grid Phase voltage	220 V
Grid frequency	50 Hz
Inductance	5 mH
Switching frequency	10 kHz

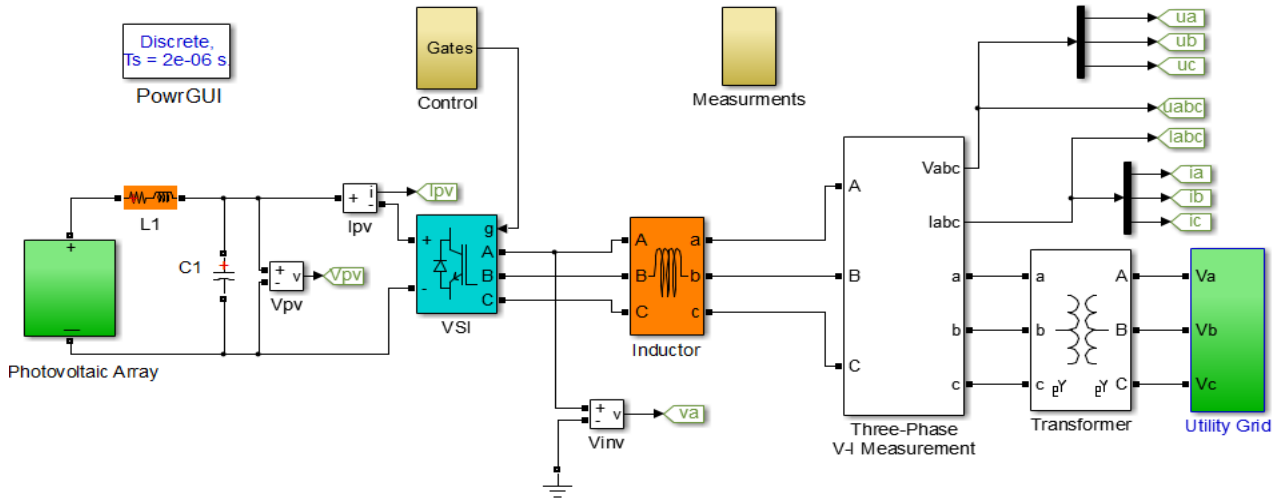

Figure 4, Simulink model of the proposed photovoltaic grid-connected system.

3.1. Steady-state response simulation results

Figures 5-10 show the response of the proposed controller at steady state. Fig. 5 shows $v_\alpha, v_\beta, v_s,$ and θ that generated from deadbeat controller. Figures 6-7 show SVM block operation. Fig. 6 shows switching times $t_1, t_2,$ and t_0 from SVM block using equations (11-13) whereas Fig. 7 shows the switching pulsed $s_a, s_b,$ and s_c that generated to switch VSI. Fig. 8 shows the inverter output phase voltage v_a and grid phase voltage u_a. Fig. 9 shows steady state simulation results for 3-phase current at the top, active power (middle plot) and reactive power (lower plot) that injected to grid for unity PF operation. Fig. 10 shows the relation between injected current and grid voltage of phase-A for unity PF. As shown in this figure, phase-A current is in phase with phase-A voltage of the grid. These waveforms confirm the proper operation of the proposed controller. As shown in these figures, the controller provides accurate regulation of injected active and reactive power to the grid for unity power factor operation.

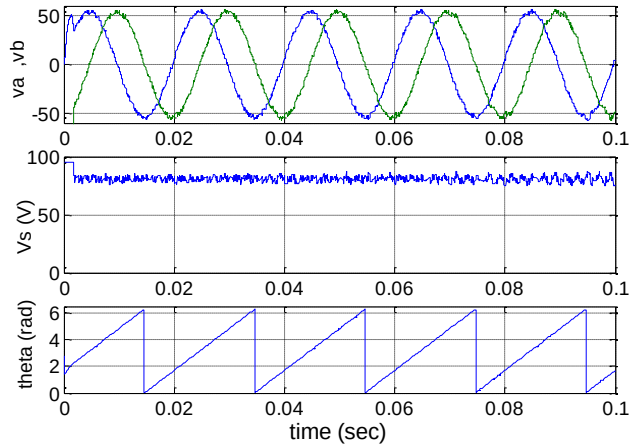

Figure 5, Simulation results at unity power factor for v_α, v_β, v_s, and θ.

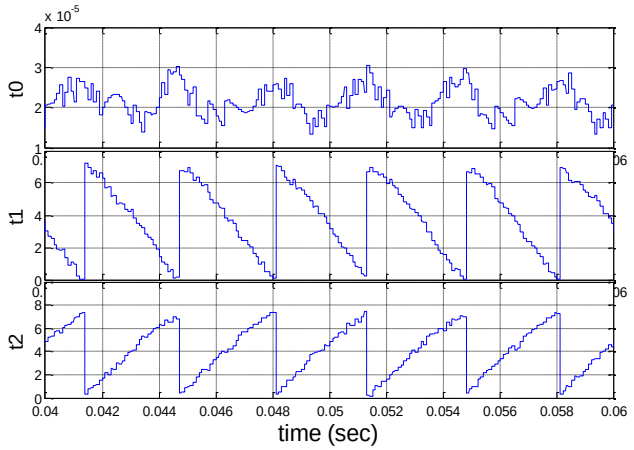

Figure 6, Simulation results for SVM calculated times, $t_0, t_1,$ and t_2.

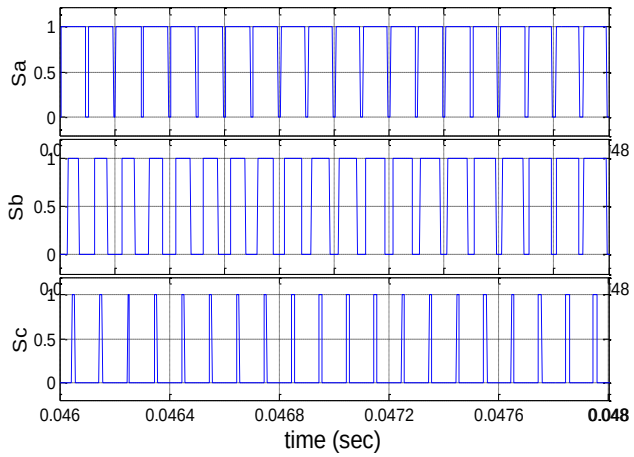

Figure 7, Simulation results for VSI gating pulses Sa, Sb, and Sc.

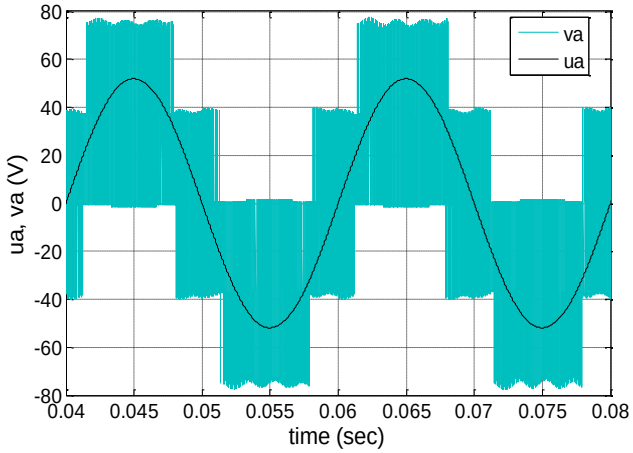

Figure 8, Simulation results for inverter voltage va, and grid voltage ua.

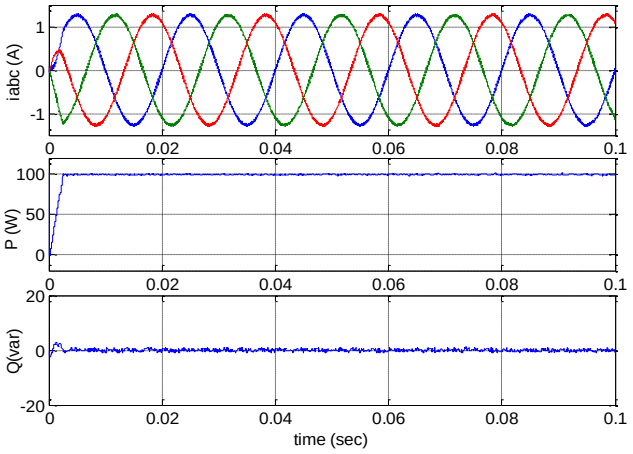

Figure 9, Steady state simulation results for 3-phase current and injected active and reactive power to grid for unity PF.

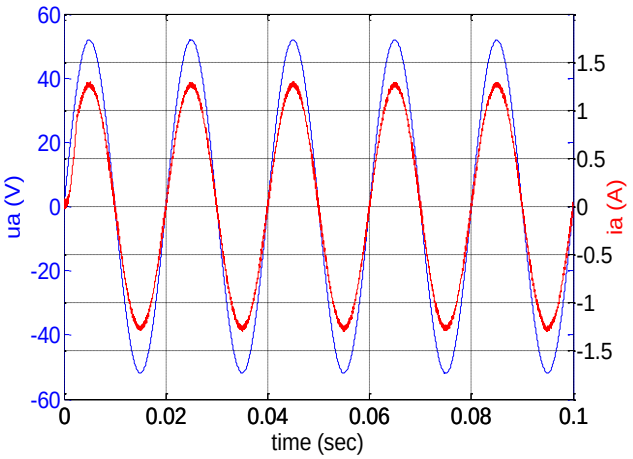

Figure 10, Steady state simulation results for phase-A grid voltage (ua) and phase-A current (ia) injected to grid for unity PF.

3.2. Transient response simulation results

Figures (11-13) show simulation results for transient state operation of the simulated system with the proposed deadbeat controller. In these figures a step change in reference active power is set and the results are recorded. Fig.11 shows step change in active power where the reactive power still at zero value and the three phase current response for this step change is recorded. The fast dynamic response of active power is clear in this figure where there is no effect on the reactive power. Also, Fig.12 shows the effect of this step change in reference active power to the values of v_α, v_β *and* $|v_s|$. The value of $|v_s|$ is slightly increases as the active power increased. Fig. 13 shows transient operation effect on phase-A current i_a and its relation with the grid phase-A voltage u_a. The fast power tracking capability of the proposed controller is clear as shown in those figures.

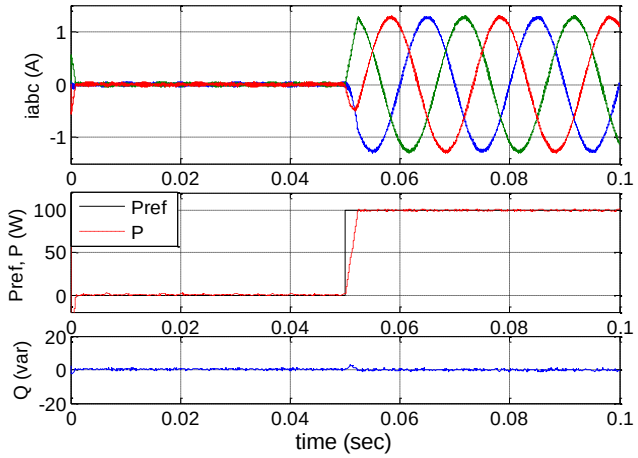

Figure 11, Transient state simulation results of 3-phase current for step change in active power.

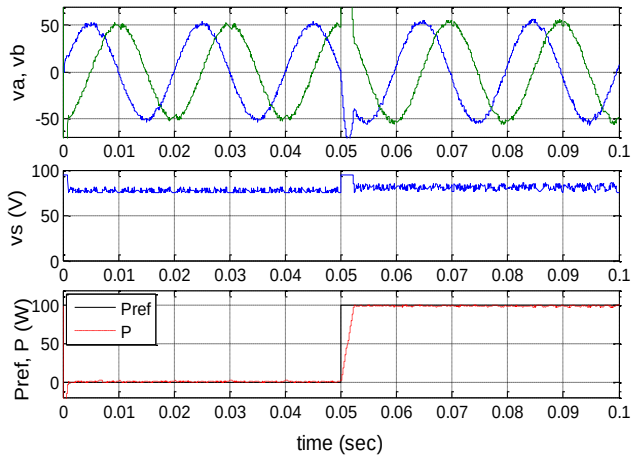

Figure 12, Transient state simulation results of v_α, v_β, v_s for step change in active power.

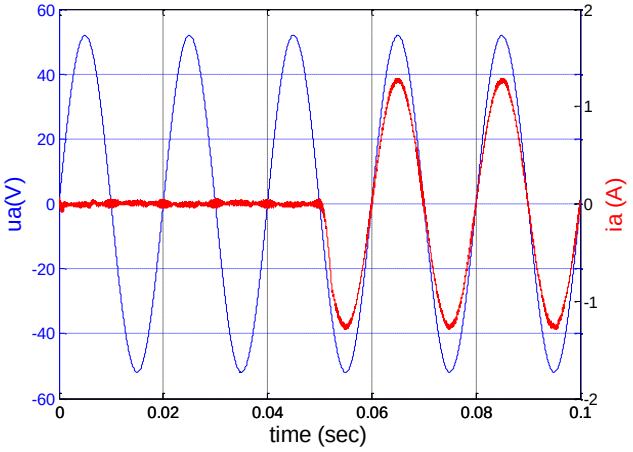

Figure 13, Transient state simulation results for phase-A grid voltage (u_a) and phase-A (i_a) injected current to grid for unity PF.

4. Experimental verification

The procedure of hardware implementation is divided into three stages;

1. Testing of system components (TSC) stage and phase sequence estimation (PSE),
2. Static mode converted stage,
3. Dynamic mode converter stage.

4.1. TSC and PSE

In this mode the different system components constructed the converter system like; System controller, Universal Inverter Module (UIM), Isolation amplifier (IA) and inductors performance were tested to be sure that it works properly. The system is integrated as shown in the following figure.

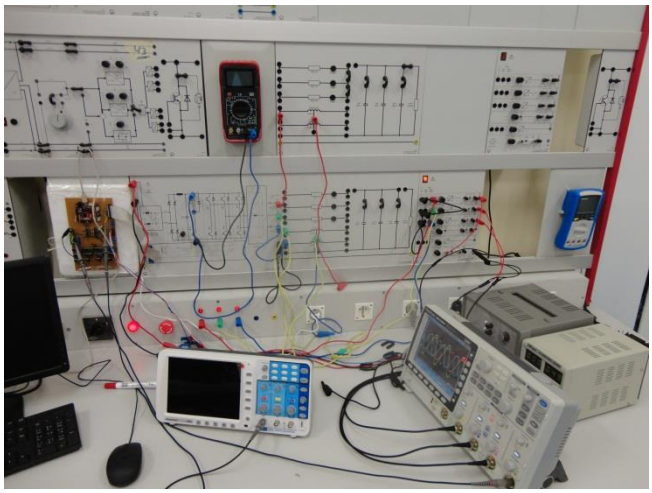

Figure 14, constructed converter system

The system controller that is Maple microcontroller is connected via a flat cable to the universal inverter module. It could be seen that gates of the six switched has a red color by means that the gates control signal are received from the microcontroller. During testing of the system components, the DC link implemented in the UIM is used instead of PV source. The output power signals of the UIM are connected to the IA via inductors. The phase sequence of the grid must be synchronized with the phase sequence of the inverter power signals. For this purpose, the grid three phase signals were presented on oscilloscope with phase A of UIM as shown in the following figure.

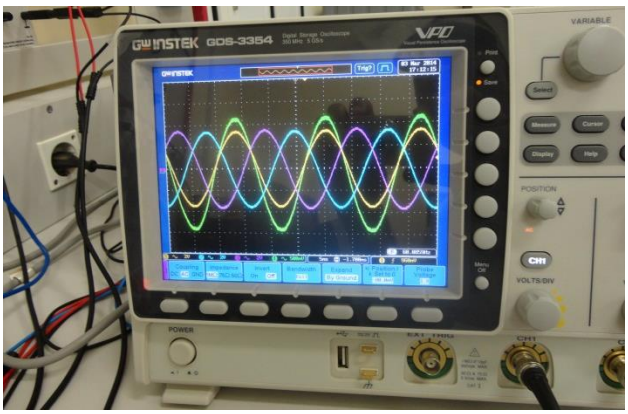

Figure 15, Phase sequence Estimation

From figure 15, it could be depicted that phase A of UIM "green color" is synchronized with utility grid phase A "yellow color", and this orientation of power wires connection is fixed in all implementation stages.

4.2. Static mode converted stage

In this mode the system operation is tested under fixed DC voltage from DC link implemented as shown in the following figure 16.

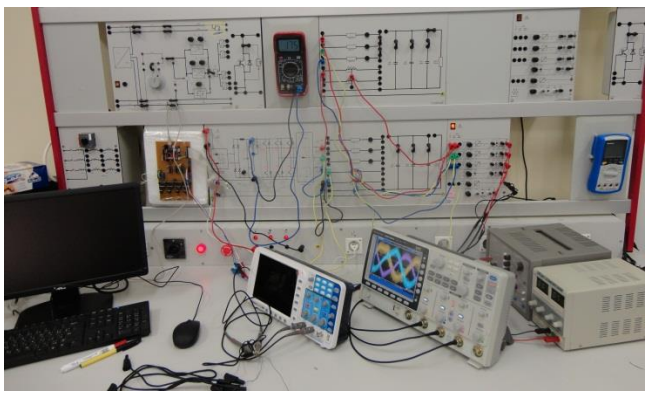

Figure 16, Static Mode Converter Testing

4.3. Dynamic mode converted stage

Grid-connected system prototype is built in the Lab. to verify the proposed power control strategy for the grid connected photovoltaic generation system. Fig.14 shows the experimental setup system.

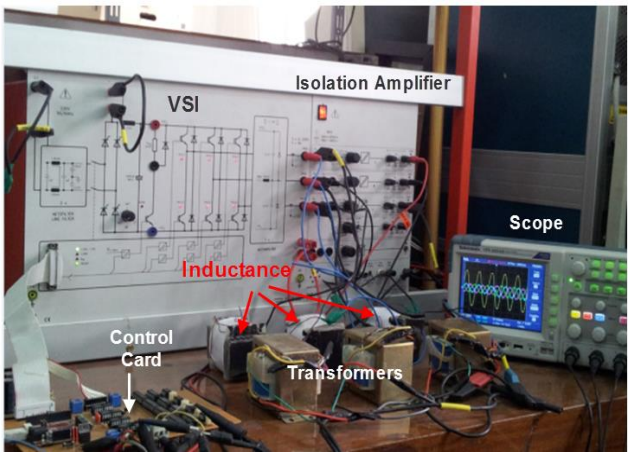

Figure 17, Experimental setup circuit.

The system is composed of 3-phase VSI, 3-phase smoothing inductance, 4-channel isolation amplifier, step-up transformers, control card, and oscilloscope. The control card is composed of 32-bit fixed-point microcontroller and signal conditioning circuit. The microcontroller advanced control timers consist of a 16-bit auto-reload counter driven by programmable prescaler [16].

It is used to generate PWM waveforms with complementary PWM output. It can be insert software dead-time between the signal and its complement. The timer also is used to generate interrupt each 100μsec for 10 kHz switching frequency of SVM. Three compare registers in the hardware timer are used to compare the computed values for three PWM values with preload register content.

The dead time is set to 3μs between each signal and its complement to prevent overlap or short circuit between upper and lower switch at the same leg of the inverter. The experimental system parameters are the same as of the simulated system that listed in Table 1.

4.1 Experimental Results

The installed PV array is shown in the following figure. It consists of 12 modules, 180W each.

During hardware implementation of experimental work, a scaled down PV system is applied to be matched with power switching, transformer and inductors rating.

Figure 18, Installed PV Array [18]

The experimental results are arranged as steady state and transient operation. The steady state results are presented to confirm the proper operation of the proposed controller. The transient operation shows the dynamics of the system for tracking changes in reference commands. The vertical scales for the experimental results will be as follows: P=100 W/div, Q=100 Var/div, u=40 V/div, i= 1 A/div.

4.1.1 Experimental steady state Results

Figs. 19-22 show experimental steady state results of the proposed grid-connected system. These figures illustrate the delivered active and reactive power to the grid, phase-A voltage and current at different cases of operation. Fig. 19 illustrates the controller output as v_α, v_β and voltage vector amplitude v_S and angle θ It is obvious that v_α and v_β are two equal and orthogonal signals.

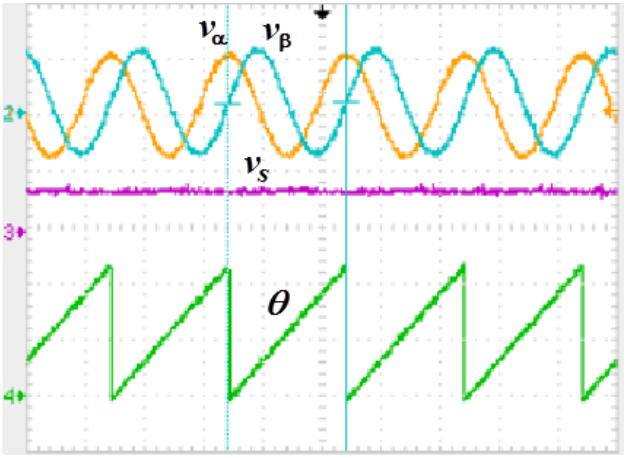

Figure 19, Calculated voltage vector components v_α, v_β , their vector amplitude v_s and angle θ, Scale: time = 20ms/div, v_α, v_β =50 V/div, v_s =100 V/div, θ = 0:2π.

Fig. 20 illustrates PWM signals for three phases of the inverter. Fig. 21 shows the 3-phase injected current to the grid and phase-A voltage of the grid. The injected phase-A current is in phase with the grid phase-A voltage u_a. This is clear in Fig. 22, where there is an active power only and reactive power that injected to the grid is set to zero. Phase-A voltage and phase-A injected current are in phase for unity power factor operation.

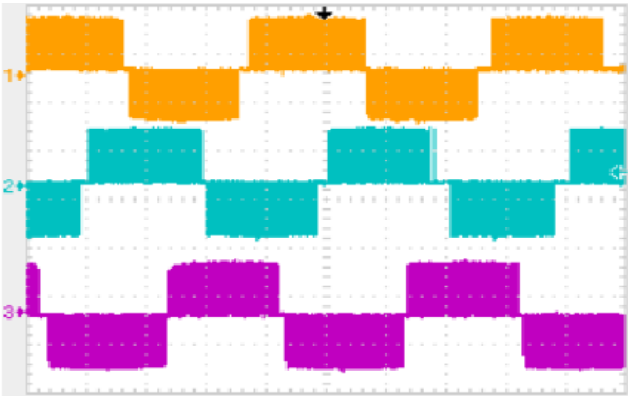

Figure 20, Microcontroller three phase PWM output signals,
Scale: time = 20ms/div, Sa, Sb, and Sc=5 V/div.

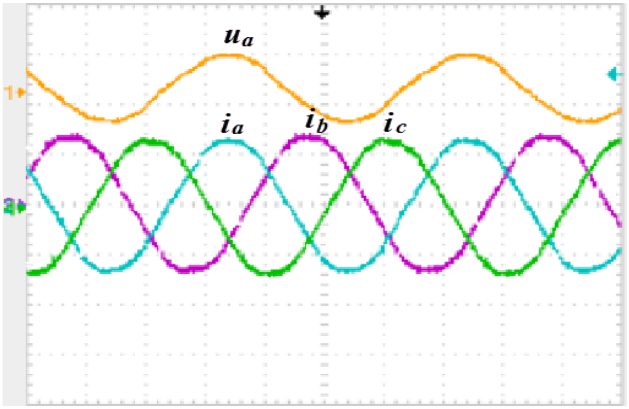

Figure 21, Experimental steady-state unity power factor operation,
Scale: time = 20ms/div, u=40 V/div, i= 1 A/div.

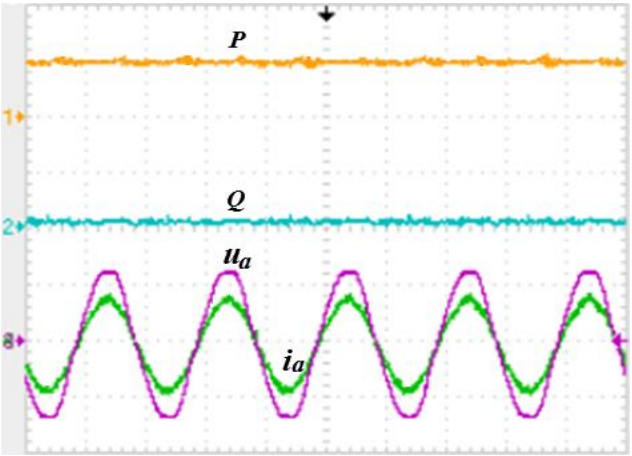

Figure 22, Experimental steady-state unity power factor operation case, Scale: time = 20ms/div, P=70 W/div, Q=70 var/div, u=40 V/div, i= 1 A/div.

4.1.2 Experimental transient response results

Fig. 23 illustrates transient response for step change in active power while no reactive power is injected. It also shows the step response of injected 3-phase current. Figures 24-25 show two cases of phase-A current step response with phase-A voltage while there is step change in active power. These figures illustrate the fast dynamic response of the system current during step change in power command.

5. Conclusion

Space vector modulation deadbeat power controller is proposed in this work. The controller is designed, simulated and implemented experimentally in α-β reference frame. The inverter voltages are deduced from the instantaneous power errors, so direct relationship between inverter voltage and required active and reactive power is found. In this technique, space vector modulation is used to generate inverter switching pulses to obtain constant switching frequency. Also, there is no need for current control loops or coordinate transformation in this technique. With the proposed strategy we gained the simplicity of the DPC technique and advantage of fixed switching frequency operations. Due to the simplicity of controller equations, a fixed-point microcontroller is used to implement the control algorithm. In the paper, simulation and experimental results for both steady state and transient operation are presented. The steady state results show that the proposed controller can provide accurate control of active and reactive power. Fast signal tracking capability of the proposed controller is illustrated by transient performance results. The experimental setup and results show that the control technique is very simple and has excellent performance.

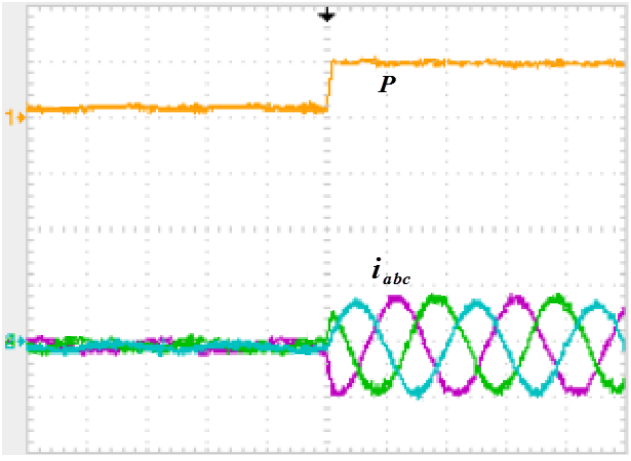

Figure 23, Experimental step-change in active power and 3-phase current response,
Scale: time = 20ms/div, P=70 W/div, i= 1 A/div.

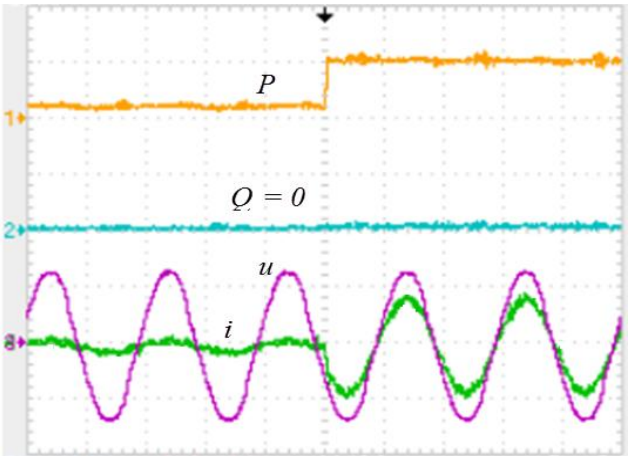

Figure 24, Step change in P while Q=0; and phase-A voltage and current relation,
Scale: time = 20ms/div, P=70 W/div, Q=70 var/div, u=40 V/div, i= 1 A/div.

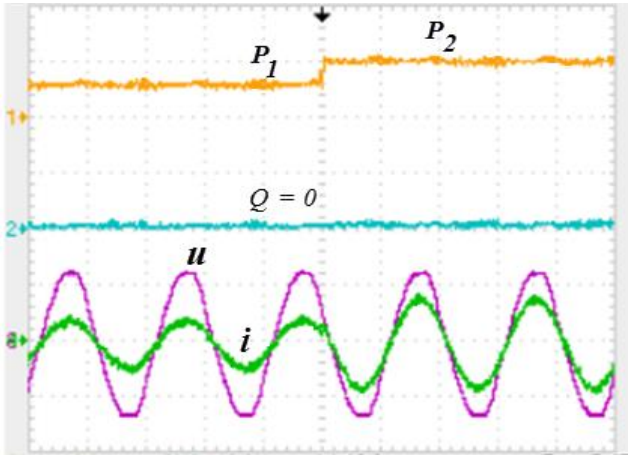

Figure 25, Step change in P while Q=0; while lower plot indicates phase-A current response,
Scale: time = 20ms/div, P=70 W/div, Q=70 var/div, u=40 V/div, i= 1 A/div.

6. Acknowledgment

The authors would like to express their thanks for the Deanship of Scientific Research in Jazan University for their support and financial agreement for this project. This paper is developed as a part of the project under title, "Simulation and Implementation of Grid-Connected Photovoltaic System" financed in the 5th program.

7. References

[1] http://www.epcor.com/efficiency-conservation/documents/distributed-generation-edmonton.pdf

[2] Yang Chen and Keyue Ma Smedley, "A Cost-Effective Single-Stage Inverter With Maximum

Power Point Tracking", IEEE TRANSACTIONS ON POWER ELECTRONICS, Vol. 19, No. 5, Sep. 2004.

[3] Sachin Jain and Vivek Agarwal , "A Single-Stage Grid Connected Inverter Topology for Solar PV Systems With Maximum Power Point Tracking", *IEEE TRANSACTIONS ON POWER ELECTRONICS*, Vol. 22, No. 5, Sep. 2007.

[4] Meral Ozarslan Yatak and Omer Faruk Bay "Fuzzy Control of a Grid Connected Three Phase Two Stage Photovoltaic System", *PROCEEDINGS OF THE 2011 INTERNATIONAL CONFERENCE ON POWER ENGINEERING, ENERGY AND ELECTRICAL DRIVES*, 2011.

[5] D. Wenlang et al. , "Modeling and Control on Grid-connected Inverter of Two-stage Matrix Converter for Direct-drive Wind Power System", *PROCEEDINGS OF THE 29TH CHINESE CONTROL CONFERENCE*, Beijing, China, July 29-31, 2010.

[6] G. Petrone, G. Spagnuolo, and M. Vitelli, "A multivariable perturb and observe maximum power point tracking technique applied to a single-stage photovoltaic inverter," *IEEE TRANS. IND. ELECTRON.*, Vol. 58, No. 1, Jan. 2011.

[7] Monfared, M. and Rastegar, H. "Design And Experimental Verification of a Dead Beat Power Control Strategy for Low Cost Three Phase PWM Converters", *INTERNATIONAL JOURNAL OF ELECTRICAL POWER & ENERGY SYSTEMS*, Vol. 42, No. 1, November 2012.

[8] Larrinaga, S., et al, "Predictive Control Strategy for DC/AC Converters Based on Direct Power Control", *IEEE TRANSACTIONS ON INDUSTRIAL ELECTRONICS*, Vol. 54, No. 3, June 2007.

[9] Bouafia, A., Gaubert, J. and Krim, F., "Predictive Direct Power Control of Three-Phase Pulsewidth Modulation (PWM) Rectifier Using Space-Vector Modulation (SVM)", *IEEE TRANSACTIONS ON POWER ELECTRONICS* Vol. 25, No. 1, 2010.

[10] Moreno, J.C., Huerta, J.M.E., Gil, R.G., and Gonzalez, S.A.,. "A Robust Predictive Current Control for Three-Phase Grid-Connected Inverters", *IEEE TRANSACTIONS ON INDUSTRIAL ELECTRONICS*, Vol. 56, No. 6, June 2009.

[11] Dragan Nesic, "Dead-Beat Control for Polynomial Systems", *Ph.D. Thesis*, Australian National University, 1996.

[12] Ma M. et al., "Study on Deadbeat Control Strategy for Grid connected Distributed Generation System", *THIRD INTERNATIONAL CONFERENCE ON ELECTRIC UTILITY DEREGULATION AND RESTRUCTURING AND POWER TECHNOLOGIES*, DRPT2008, Nanjing China, April 2008.

[13] Atia Y., Salem M., "Analysis and Design of Improved Predictive Direct Power Control Strategy for Renewable Energy Grid-Connected Systems", *3RD INTERNATIONAL CONFERENCE ON ADVANCED CONTROL CIRCUITS AND SYSTEMS (ACCS'013)* 30 Nov. – 03 Dec, Luxor, Egypt, 2013.

[14] Krause P.C., "Analysis of Electric Machinery", *Mc.Graw-Hill*, USA, 1986.

[15] Salem M, and Atia Y., "Design and Implementation of Predictive Current Controller for Photovoltaic Grid-Tie Inverter", *WSEAS TRANSACTIONS ON SYSTEMS AND CONTROL*, Volume 9, 2014.

[16] Reference Manual RM0008 (PDF); definitive resource for peripherals on the STM32F1 line, http://www.st.com.

[17] Mohamed Zahran, M.M. Salem and Yousry Atia, "Active Anti-Islanding Based Inverter for PV Grid Connected System", IPASJ *INTERNATIONAL JOURNAL OF ELECTRICAL ENGINEERING* (IIJEE), Volume 2, Issue 9, September 2014.

[18] Mohamed Zahran and Ali M. Yousef, "Monitoring of Photovoltaic Wind-Turbine Battery Hybrid System", *WSEAS TRANSACTION ON POWER SYSTEM*", Issue 1, Volume 9, January 2014.